



## Study on selective adsorption and separation of dysprosium by a multi-template oriented imprinted composite membrane

Wenda Wang\*, Jiachen Yuan, Yue Jiang, Weiqiao Liu

*School of Chemical and Environmental Engineering, Jiangsu University of Technology, Changzhou 213001, 1801 Zhongwu Avenue, Wujin District, Changzhou, Jiangsu, PR China, emails: dada1986121300@163.com (W. Wang), yuanjiachen0330@163.com (J. Yuan), jiang991013@163.com (Y. Jiang), lwq@jsut.edu.cn (W. Liu)*

Received 7 September 2020; Accepted 6 May 2021

---

### ABSTRACT

Dysprosium (Dy) ion has received widespread attention in industrial applications due to its unique physical and chemical properties. The potential economic value of adsorbing and separating rare earth Dy ions from waste permanent magnets is high. We use graphene oxide as the material to prepare the membrane for selective adsorption of Dy. Graphene oxide has high stability, its structure is two-dimensional plane, and it has high acid and alkali resistance. At suitable pH conditions, the prepared membranes can have high selective adsorption properties to Dy ions by ionic imprinting. A series of studies on the effects of various pH on the adsorption effect, isotherm, kinetics, and competitive adsorption and so on were carried out. The model of selective adsorption of Dy ions was proposed to obtain membrane materials with good selectivity and good separation. We found that at pH = 5.0, the adsorption performance of the membrane for Dy ions was the best, and the adsorption reached equilibrium after 2 h of adsorption. The maximum adsorption amount reached 26.27 mg g<sup>-1</sup>. The membrane has high acid resistance and high adsorption selectivity to Dy ions.

*Keywords:* Adsorption; Dysprosium; Multi-template; Imprinting; Membrane

---

### 1. Introduction

Rare earth elements (REEs) were first separated in 1794. There are 17 kinds of metal elements, which are divided into heavy rare earth and light rare earth. Demand for rare earth elements has increased dramatically in recent decades, as they are one of the indispensable elements in key technologies such as wind turbines and electric vehicle engines [1,2]. Rare earth elements are widely used in many fields. In energy storage systems, rare earth can be used as electrodes in lead batteries and can effectively prevent battery corrosion. Where dysprosium (Dy) can be used as a phosphor activator in luminescent materials, which makes Dy have a great prospect market [3,4].

Dy ions are used in many fields, such as lasers, computer hard disks, nuclear reactors. Dy ions are particularly important in national defense construction and weapon

manufacturing, especially in the manufacture of some precision weapons. It is precisely because Dy ions are so important that the current demand is also increasing. China is a major exporter of dysprosium. They go abroad to Japan and Korea in the form of dysprosium oxide every year. However, due to environmental pollution and resource control, China has begun to restrict the export of dysprosium. So, we need a stable and reliable source of ions. The most likely solution now is to recycle Dy ions from scrap magnets, but global REEs recycling is low (<1%). These waste magnets also pollute the earth's environment at the same time. Therefore, magnet recovery is a feasible alternative to mining Dy. Therefore, many scholars have put forward more methods to extract Dy [5,6]. With the wide use of rare earth elements and rare earth products in recent years, rare earth elements will inevitably enter groundwater, rivers and other water systems in

---

\* Corresponding author.

various ways. When rare earth elements enter the atmosphere, they will then enter rivers in the form of rainfall. After infiltration into groundwater, ultimately affecting the food chain, human health harm. In the process of mining some rare earth mines, the industrial wastewater treatment is unreasonably infiltrated into the surrounding farmland and pasture water system, which leads to the toxicity of crops, the decrease of production and the slow development of livestock [7,8]. A small amount of rare earth elements can promote the growth of plants in the soil, but too much rare earth elements can inhibit the growth of crops.

It is precisely because these rare earth solid wastes contain a variety of useful rare earth elements. If we do not treat them effectively, these solid wastes will also pollute the environment. Therefore, how to separate these useful rare earth elements has become a problem to be discussed in this paper. Smith et al. [9] studied the adsorption properties of carbon black oil on aqueous mixtures of light rare earth elements (Y, La, Ce, Nd and Sm) and then compared this adsorption material with recycled tire carbon black and other commercial and functionalized carbon. In addition, Sun et al. [10] have also developed a rare earth separation method, which uses carbonized polydopamine nano carbon shells as materials to adsorb and separate rare earth ions [10]. In their study, polydopamine was first carbonized to produce carbon nanoshells, and the structure effect of carbon nanoshells was used to adsorb REEs. Sun et al. [10] also compared the effects of carbon nanoshells and solid carbon spheres on the adsorption properties of REE rare earths. They prepared solid carbon spheres with 60 nm carbon shells and 500 nm carbon shells. Finally, it was found that the adsorption performance of carbon nanoshells to REE is much better than that of solid carbon spheres. They believe that the specific surface area, pore structure and amine and carbonyl groups from the grafted dopamine lead to good adsorption properties of the carbon nanoshells.

Silicon-based material is an ideal material for loading materials used for modification. It also brings the possibility of porosity and specific surface area of adsorption materials [11–13]. Many methods can be adopted for preparing modified silicon films, such as chemical fixation. A silane coupling agent can be used as a precursor to providing stable support for further modification of subsequent materials because it can form stable chemical bonds (Si–O) [12,14]. Ion imprinted membrane is to use metal ions as templates, metal ions and functional monomers plus complexing agents, the three will be combined by ligand action, the template after elution, metal ions will be eluted, will leave holes, These holes are similar in size to metal ions, so that these holes will form imprinting sites [15,16]. By studying these papers and referring to many methods of separation of rare earth elements, we propose to use bio-templated cellulose nanocrystals (CNCs) as structure-oriented templates [17,18]. The ions Dy the imprinted template can form a whole with the template, and the Dy ions and cellulose can be removed by pickling, so that the whole surface of the membrane will be covered with imprinted sites with special adsorption properties for Dy ions [19].

Due to some unique properties, ion-imprinted polymers (IIPs) have shown great potential to identify various analytes from small molecules to large molecules. But there are some drawbacks because IIP lack electrical conductivity and electrocatalytic activity, which may potentially limit their applications in the sensor field. To improve its analytical performance and overcome these shortcomings in chemical sensors, different carbon nanotubes, graphene oxide (GO), carbon electrodes and carbon dots are combined with IIP and magnetic IIP [20]. In order to improve its analytical performance.

In this paper, we use graphene oxide as the material to prepare the membrane. Graphene oxide has high stability, its structure is two-dimensional plane, and it has high acid and alkali resistance. At suitable pH environment conditions, the prepared membranes can have high selective adsorption properties to Dy ions by ion imprinting. A series of studies on the effects of various pH on the adsorption effect, isotherm, kinetics, competitive adsorption and so on were carried out. The model of selective adsorption of Dy ions was proposed to obtain membrane materials with good selectivity and good separation. A study will be carried out on the adsorption and adsorption selection of Dy ions by non-imprinted and imprinted membranes.

## 2. Experimental section

### 2.1. Experimental materials and reagents

Analytical pure reagent tetraethyl orthosilicate (TEOS) purchased from Aladdin Chemical Reagent Co., Ltd., (Shanghai). Graphene oxide aqueous solution purchased from Suzhou Carbon Fung Technology Company (2 mg mL<sup>-1</sup>). Glucose, concentrated sulfuric acid (98% concentration) and dysprosium oxide and other compounds purchased from Shanghai Chemical Reagent Co., Ltd. Medical degreasing cotton (Robust Medical Supplies Co., Ltd).

### 2.2. Instruments and equipment

The morphological characteristics of the samples were characterized by scanning electron microscopy (SEM; Hitachi S-4800). Test sample surface functional groups need to be used to Fourier-transform infrared spectrometer (FT-IR, Nexus 470, USA). The pH value of the solution is measured using a Digital Acidometer (PHS-3C, Shanghai Instrument, China). A specific surface area analyzer is used to test the mesoporous pore properties of the samples (D-35614 Asslar Instruments, Germany). Inductively coupled plasma emission spectrometers are needed when we need to measure the concentration of rare earth ions in the solution (ICP-MS, Varian, USA). When we need to do a thermogravimetric analysis of the sample, we need to use the integrated thermal analyzer (STA 449C, Germany). Make CNCs need to use the JJ-1A digital display force electric agitator. Kitt TG16G centrifuge for centrifuge CNCs solution. A SHA-A water bath constant temperature oscillator (made by Tianjin Sedlis) and a PTFE disc for dialysis.

### 2.3. Preparation of materials

#### 2.3.1. Preparation of CNCs

At a temperature of 45°C, the beaker was stirred with an agitator for 2 h with a mixed solution of cotton wool and sulfuric acid. After completion, add cold deionized water to the solution to terminate the hydrolysis, add about 1,500 mL of cold deionized water, rest overnight, and then pour out the supernatant and repeat the process three times. Then the solution was centrifuged. CNCs obtained after centrifugation was put into the dialysis membrane bag for dialysis, and the water in the beaker was changed every 12 h. When the pH value was equal to 2.4, the CNCs solution was ultrasound every time, the time was 10 min.

#### 2.3.2. Preparation of multi-template guided ion-imprinted graphene oxide composite film

0.4 mL of TEOS was added to the 7.5 mL of CNCs solution. Then add 0.1 mL of 3-acetyloxypropyl trimethoxy

silane, 8 mg of dysprosium nitrate into the solution, Finally, a mass percentage of 0%, 1%, 5% of graphene oxide added to the solution. Reaction of the solution system at 60°C for 2 h. After the reaction is finished, the solution is put into a PTFE disc and dried at room temperature to form a film so that the IGOMs can be prepared. Preparation of graphene oxide imprinted film (NIGOMs) is same as (IGOMs) without adding dysprosium nitrate into the solution.

The solution preparation of adsorption experiment: all the reserve solutions are prepared by the corresponding rare earth nitrate and diluted to different concentrations in the specific use process.

## 3. Results and discussion

### 3.1. Material characterization

We performed a series of characterizations for IGOMs and NIGOMs. Under SEM, morphology of IGOMs and NIGOMs were observed. The scanning photos of IGOMs and NIGOMs are shown in Fig. 1. It can be found that

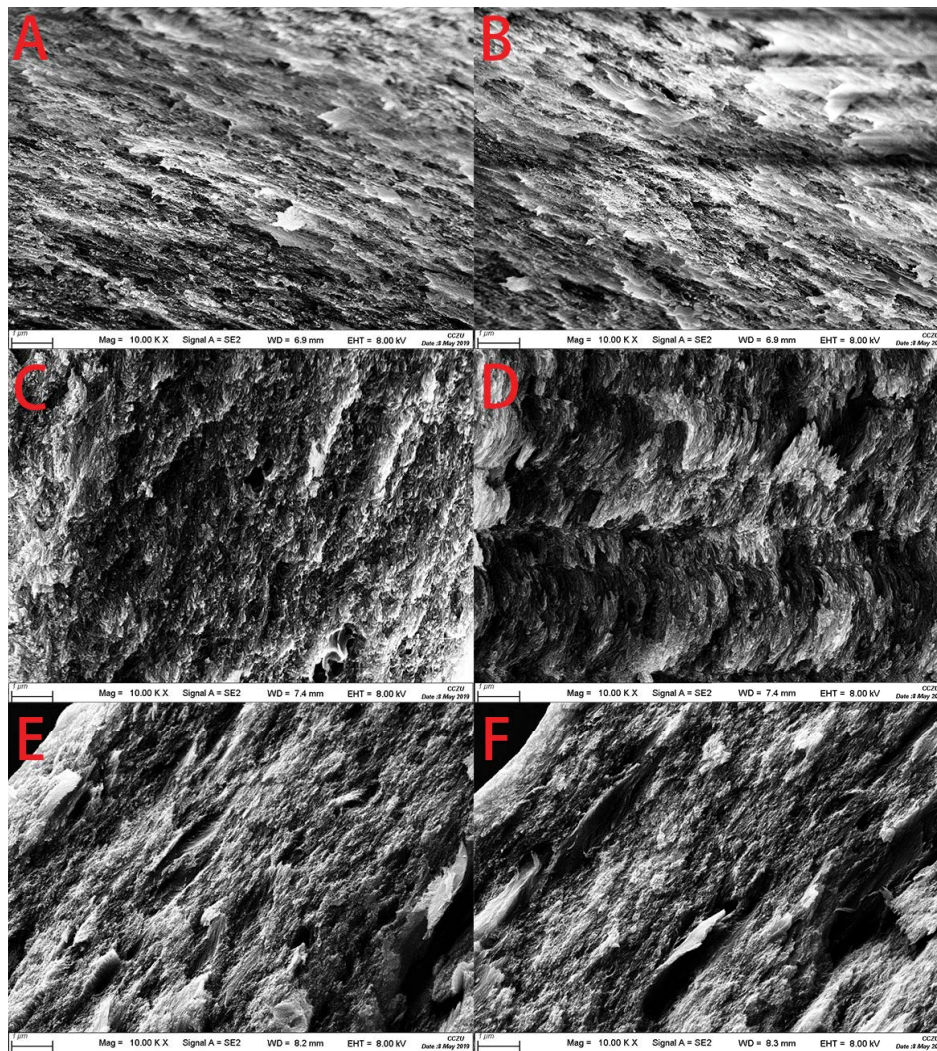


Fig. 1. Scanning electron microscopy image of IGOMs and NIGOMs, (A, B) for the wt-0%-GO IGOMs and NIGOMs, (C, D) for the wt-1%-GO IGOMs and NIGOMs (E, F) wt-5%-GO IGOMs and NIGOMs.

the structure of membranes in the figure is a sheet, which indicates that the membrane we prepared is a chiral liquid crystal sequence structure, which also confirms our successful preparation of multi-template guided ion imprinted graphene oxide film.

Fourier-transform infrared spectra of IGOMs and NIGOMs are shown in Fig. 2. The absorption characteristic peak at 1,059  $\text{cm}^{-1}$  is due to the asymmetric stretching vibration of the Si–O–Si, the peak at 1,654.8  $\text{cm}^{-1}$  is due to C–O–C stretching, the absorption peak of vibration in the 2,923.81  $\text{cm}^{-1}$  region is caused by Si–OH hydroxyl stretching vibration, the standard peak at 3,422  $\text{cm}^{-1}$  is due to the stretching vibration of –NH<sub>2</sub> and –OH.

Under the condition of nitrogen protection, we have carried on the thermogravimetric analysis to the IGOMs and NIGOMs, processed, analyzed and drawn the thermogravimetric analysis diagram TGA, as shown in Fig. 3. The temperature increased from 0°C to 800°C, from 0°C to 100°C, the weight loss of imprinted membrane was about 7%, and the weight loss of non-imprinted membrane was about 15%. This temperature interval mainly reduced the crystalline water in the membrane, indicating that the prepared membranes all had good hydrophilicity, which provided good conditions for the adsorption of Dy ions in aqueous solution. Between 130°C and 800°C, the total weight of the imprinted film was reduced by about 45%, and the weight of the non-imprinted film was reduced by about 38%. The thermogravimetric analysis curve of the imprinted film was above the thermogravimetric analysis curve of the non-imprinted film, indicating that the imprinted film had better thermal stability than the non-imprinted film.

### 3.2. Adsorption test

#### 3.2.1. pH impact

PH is the key factor affecting the recovery rate in the process of recovering Dy ions, because the leaching solution of magnetic alloys in the second phase is always highly

acidic, so we chose pH = 1.0 to 7.0 to study the adsorption properties of IGOMs and NIGOMs. Fig. 4 shows the effect of pH on the adsorption properties of IGOMs and NIGOMs, and the effect of imprinting factor (10 mL of Dy ions with 50 mg L<sup>-1</sup>). We can see from the pH diagram

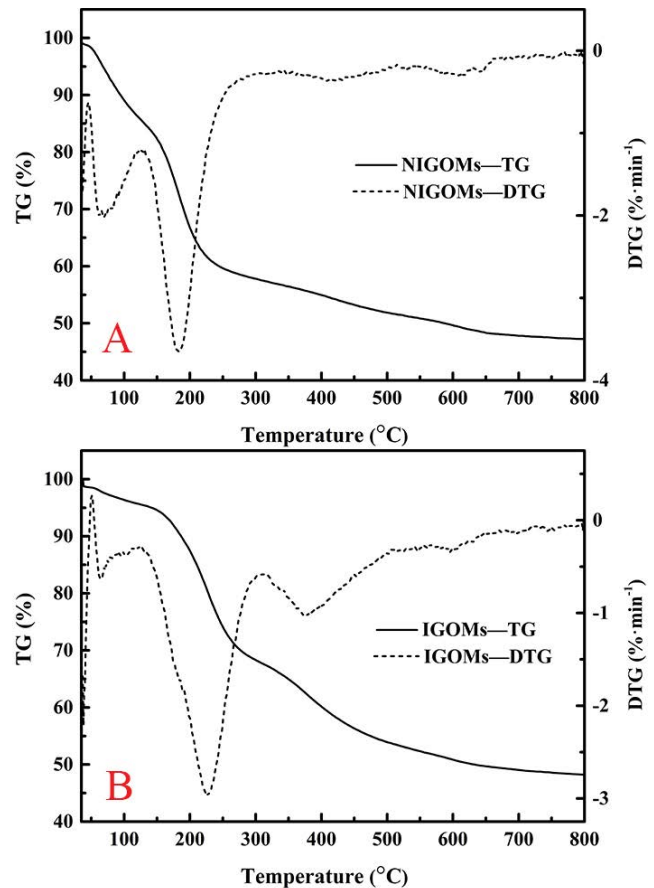


Fig. 3. Thermogravimetric diagram of (A) NIGOMs and (B) IGOMs.

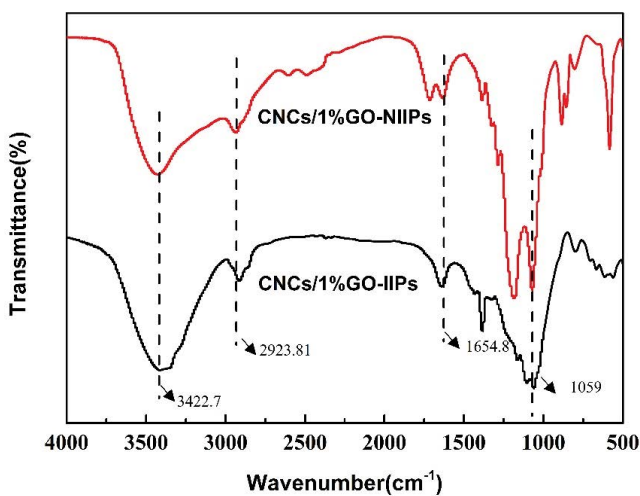


Fig. 2. Fourier-transform infrared spectra of IGOMs and NIGOMs.

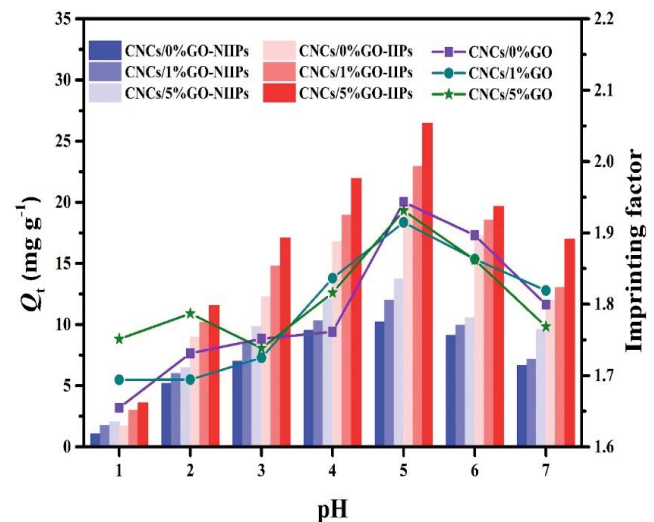


Fig. 4. Effect of pH on adsorption capacity.

that the adsorption properties of NIGOMs and IGOMs to Dy ions are increasing with the increase of pH, and the adsorption properties of Dy ions are higher than that of graphene oxide. The adsorption properties of imprinted and non-printed films will increase. The pH is not the bigger the better. Fig. 4 shows that when the pH reaches 5.0, both the IGOMs and NIGOMs reach the maximum adsorption capacity, and the adsorption capacity decreases gradually with the increase of 5.0. The added graphene oxide also reaches the maximum adsorption capacity at a mass ratio of 5.0 and this also indicates that our prepared membranes have strong acid resistance, and the subsequent adsorption experiments will also be carried out under the condition of pH = 5.0.

### 3.2.2. Adsorption kinetics

To further study the adsorption properties of IGOMs and NIGOMs, we carried out experiments on adsorption kinetics. By the change of time to study the adsorption of Dy ions. Eq. (1) represents the amount of adsorption in a certain period of time.

$$Q_t = \frac{V(C_0 - C_t)}{W} \quad (1)$$

where  $Q_t$  ( $\text{mg g}^{-1}$ ) represents the amount of Dy ions adsorbed by the membrane,  $C_0$  ( $\text{mg L}^{-1}$ ) represents the concentration of Dy ions in the solution before adsorption, while  $C_t$  ( $\text{mg L}^{-1}$ ) represents the concentration of Dy ions in the solution after adsorption for a certain time period, and the volume of the adsorbed solution. We select 10 mL, in this experiment and  $W$  the mass of the film we added in the experiment. In this experiment, we add 10 mg at the same time. On the other hand, we use the pseudo-first-order kinetic model (PFOKM) and pseudo-second-order kinetic model (PSOKM) to fit the kinetic models of imprinted and non-printed films, where the nonlinear forms of PFOKM and PSOKM are Eqs. (2) and (3), respectively.

$$Q_t = Q_e - Q_e e^{-k_1 t} \quad (2)$$

$$Q_t = \frac{k_2 Q_e^2 t}{1 + k_2 Q_e t} \quad (3)$$

Finally, we draw a diagram of the adsorption kinetics of IGOMs and NIGOMs by fitting. Fig. 5 shows the comparison of adsorption capacity and kinetic fitting of NIGOMs and IGOMs at 298.15 K, pH = 5.0 and 50  $\text{mg L}^{-1}$ , and the contrast between the materials after adding different proportions of GO. The adsorption rate of the CNCs/5% GO-IIPs can be clearly seen from Fig. 5, for example, the adsorption amount of 6.862  $\text{mg g}^{-1}$  was generated within 30 min after the adsorbent was added to the simulated sample. The adsorption capacity increased rapidly between 0–200 min and the adsorption was slow after 200 min and finally reached the adsorption equilibrium at 410 min. We can see from Fig. 5A–C

that the adsorption capacity of the film after doping three kinds of graphene oxide with different the best CNCs/5%GO-IIPs, followed by CNCs/1%GO-IIPs and CNCs/0%GO-IIPs. This is because there is a strong force between the molecular chains of natural polysaccharide cellulose itself, resulting in fast adsorption efficiency.

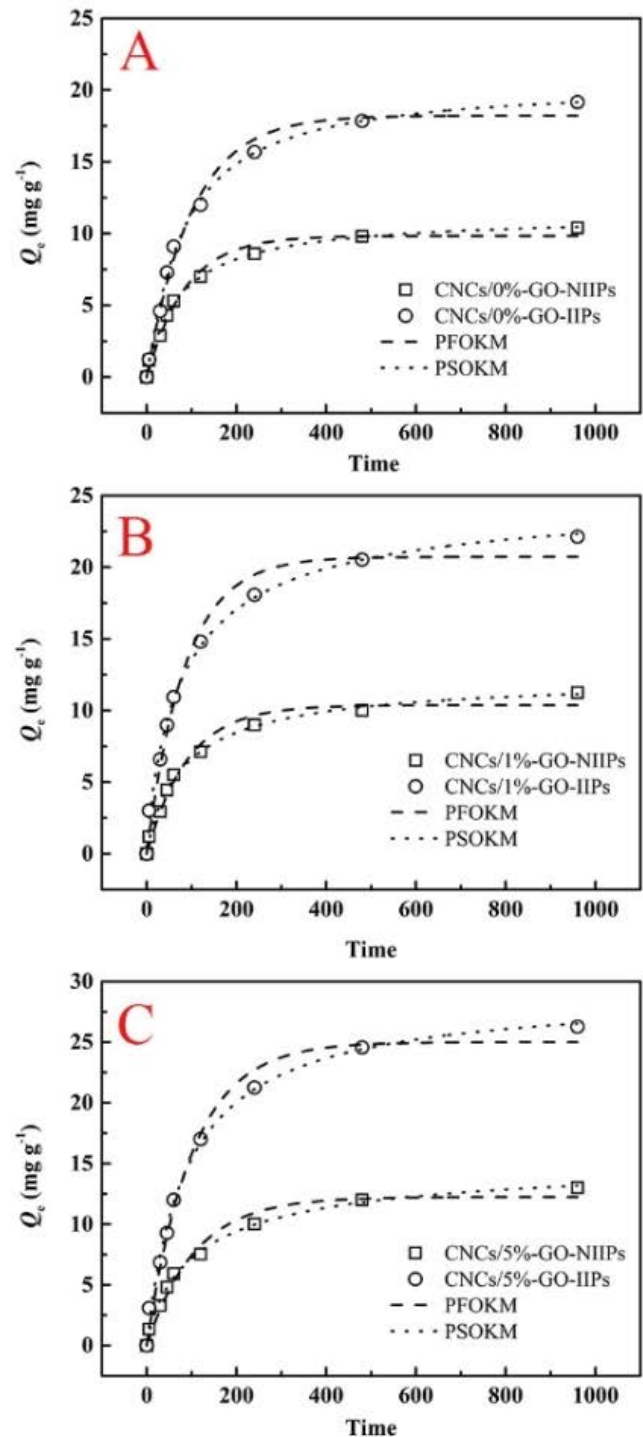


Fig. 5. (A) For CNCs/0%GO-NIIPs and CNCs/0%GO-IIPs, (B) for CNCs/1%GO-NIIPs and CNCs/1%GO-IIPs and (C) for CNCs/5%GO-NIIPs and CNCs/5%GO-IIPs, the dynamic diagram.

Secondly, graphene oxide has a lot of oxygen functional groups to help adsorption while its lamellar structure helps to expand the specific surface area of the material. We can see from Fig. 5A–C that the adsorption performance of IGOMs is better than that of NIGOMs regardless of the doping amount. It can be seen that the material IGOMs is more in line with the quasi-second-order kinetic equation, indicating that the adsorption mode is more in line with chemisorption, and it is not easy to desorb between molecules by chemical bond. The relevant data of dynamic fitting are shown in Table 1.

### 3.2.3. Adsorption isotherms

The adsorption isotherms of IGOMs and NIGOMs were fitted to further explore the adsorption Dy ion properties of IGOMs and NIGOMs. Fig. 6 shows the comparison of the adsorption isotherm fitting between NIGOMs and IGOMs at 298.15 K, pH = 7. The isotherm model can better explain the data of the sample and better explain the adsorption performance of the membrane. The fitted line shows that the imprinted sites are uniformly distributed on the whole membrane, which is consistent with the trend of the isotherm. Therefore, it is also possible that the adsorption mode of the membrane prepared in this experiment is the chemical adsorption of monolayer, and there is no interaction between the adsorption molecules. CNCs/0%GO-NIIPs, CNCs/0%GO-IIPs, CNCs/1%GO-NIIPs, CNCs/1%GO-IIPs, CNCs/5%GO-NIIPs. The correlation coefficients ( $R^2$ ) between CNCs/5%GO-IIPs and Langmuir isotherms were 0.992, 0.994, 0.992, 0.993, 0.999 and 0.995. With the increasing concentration of adsorption solution, the adsorbent gradually reaches adsorption saturation. The addition of the maximum adsorption capacity of IGOMs material is  $46.5 \text{ mg g}^{-1}$ , GO and the structural characteristics of the CNCs itself have a great influence on the adsorption capacity. Other adsorption fitting data are shown in Table 2. Moreover, the adsorption ion affinity of the adsorption membrane represented by the  $R_L$ ,  $R_L$  ( $0 < R_L < 1$ ) can be obtained by calculation, in which the smaller the value of the  $R_L$  more favorable the adsorbent adsorption is. Table 2 shows that the  $R_L$  value of graphene IGOMs adding 5% mass ratio is much less than that of graphene with 5% mass ratio of 0.966, which indicates that the hydrophilicity of IGOMs is better. It confirms that IGOMs is more favorable for the adsorption

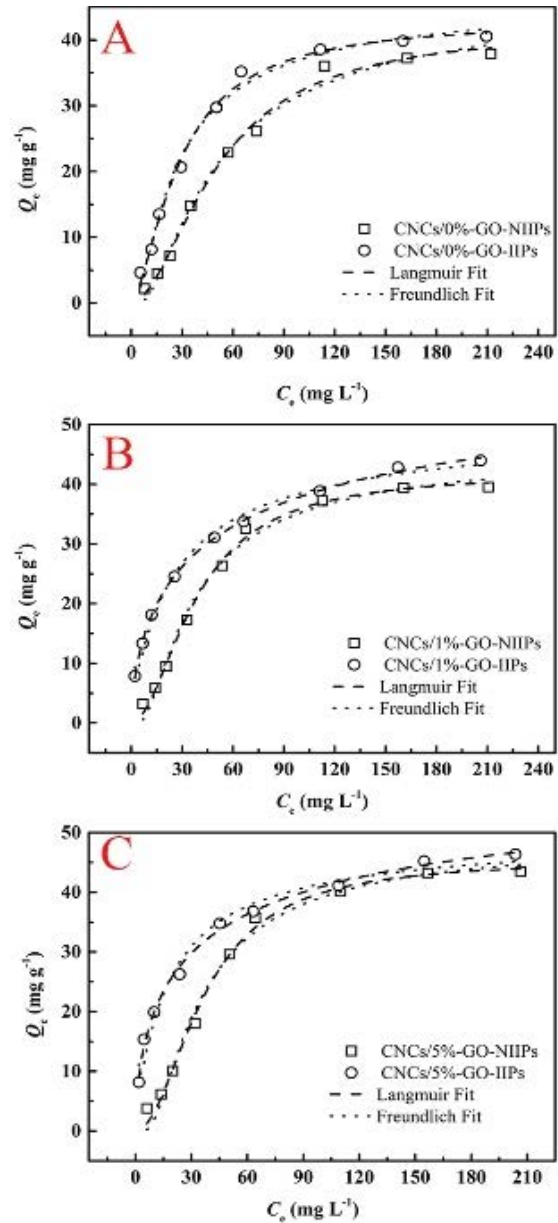


Fig. 6. Isotherm diagrams IGOMs and NIGOMs, (A) for the wt-0%-GO IGOMs and NIGOMs, (B) for the wt-1%-GO IGOMs and NIGOMs, and (D) for wt-5%-GO IGOMs and NIGOMs.

Table 1  
Kinetic constants for the quasi-first-order and quasi-second-order models

Sample	$Q_{e,exp}$ ( $\text{mg g}^{-1}$ )	Quasi-first-order kinetic equation			Quasi-second-order kinetic equation				
		$Q_{e,e}$ ( $\text{mg g}^{-1}$ )	$k_1$ ( $\text{L min}^{-1}$ )	$R^2$	$Q_{e,e}$ ( $\text{mg g}^{-1}$ )	$k_2 \times 10^{-2}$ ( $\text{g mg}^{-1} \text{min}^{-1}$ )	$h$ ( $\text{mg g}^{-1} \text{min}^{-1}$ )	$t_{1/2}$ (min)	$R^2$
CNCs/0%GO-NIIPs	10.40	9.837	0.0116	0.985	11.298	0.127	1.43484	7.874	0.993
CNCs/1%GO-NIIPs	11.25	10.368	0.0111	0.978	12.405	0.143	1.77391	6.993	0.991
CNCs/5%GO-NIIPs	13.02	12.243	0.0093	0.976	15.41	0.117	1.80297	8.547	0.994
CNCs/0%GO-IIPs	19.15	18.227	0.01	0.989	20.49	0.043	0.88107	23.25	0.996
CNCs/1%GO-IIPs	22.13	20.725	0.012	0.979	24.98	0.087	2.17326	11.49	0.992
CNCs/5%GO-IIPs	26.27	25.007	0.0099	0.987	29.12	0.042	1.22304	23.81	0.992

Table 2  
Adsorption equilibrium constants for Langmuir and Freundlich isotherm equations

Adsorbents	Langmuir				Freundlich	
	$R^2$	$K_L \times 10^{-2}$ (L mg <sup>-1</sup> )	$Q_m$ (mg g <sup>-1</sup> )	$R_L$	$R^2$	$K_F$ (mg g <sup>-1</sup> )
CNCs/0%GO-NIIPs	0.992	0.077	41.70	0.966	0.988	46.81
CNCs/1%GO-NIIPs	0.994	0.106	41.92	0.953	0.987	45.37
CNCs/5%GO-NIIPs	0.992	0.075	45.37	0.966	0.984	48.56
CNCs/0%GO-IIPs	0.993	0.587	43.05	0.788	0.987	46.21
CNCs/1%GO-IIPs	0.999	8.437	63.94	0.206	0.989	51.34
CNCs/5%GO-IIPs	0.995	11.46	63.07	0.160	0.968	50.16

of Dy ions among which CNCs/5%GO-IIPs is the most favorable adsorbent.

The equations of Langmuir and Freundlich isotherms are represented by Eqs. (4) and (5), respectively.

$$Q_e = \frac{K_L Q_m C_e}{1 + K_L C_e} \quad (4)$$

$$Q_e = K_F C_e^{1/n} \quad (5)$$

where  $Q_m$  (mg g<sup>-1</sup>) represents the maximum adsorption capacity of the membrane,  $K_L$  (L g<sup>-1</sup>) and  $K_F$  (mg g<sup>-1</sup>) represent the affinity constant of the Langmuir isotherm and the direction constant of the Freundlich isotherm, respectively.  $1/n$  represents the heterogeneity factor. Eq. (6) represents the  $R_L$  to analyze the advantages of adsorption by the  $R_L$  of separation factors.

$$R_L = \frac{1}{1 + C_m K_L} \quad (6)$$

where  $C_m$  is the maximum initial value of the Dy(II) concentration.

### 3.2.4. Competitive adsorption experiments

For the purpose of studying the adsorption selectivity of the prepared membrane to Dy ions under the environment of coexistence of various homologs, we added four ions to the solution, Dy ions, Nd ions, Gd and Fe ions. Adoption of  $K_d$ ,  $K$  and  $K'$  (distribution factors, selectivity coefficient and relative selectivity coefficient) to compare the selective adsorption properties of IGOMs and NIGOMs to Dy ions.  $K_d$ ,  $K$  and  $K'$  formulas are as follows:

$$K_d = \frac{C_0 - C_f}{C_f} \times \frac{V}{m} K = \frac{K_{d1}}{K_{d2}} \quad (7)$$

$$K' = \frac{K_{3D-MICF}}{K_{3D-MNCF}} \quad (8)$$

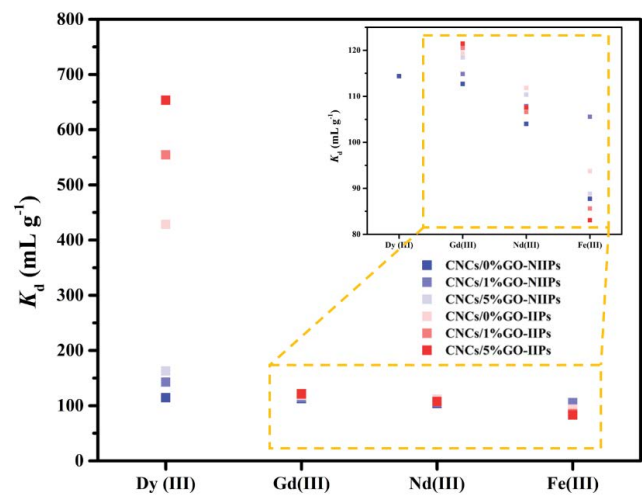


Fig. 7. Selectivity test of IGOMs and NIGOMs.

where  $C_0$  represents the initial concentration of 4 ions (50 mg L<sup>-1</sup>) and  $C_f$  represents the final concentration of each ion. A relative selectivity coefficient  $K'$  represents the magnitude of the affinity between the selective imprinting sites of the material and the template ions. We can see from Fig. 7 that the  $K_d$  value of imprinted film is obviously higher than that of non-imprinted film, and the  $K_d$  value increases with the increase of graphene oxide.  $K_d$  values of imprinted membranes are so high because of silane, cellulose, and metal ions. Graphene oxide forms a whole structure under chelation. Finally, by acid elution, the eluent uses 50% sulfuric acid to completely elute the metal ions and cellulose, and finally forms the imprinted hole position with specific adsorption effect on the Dy ions. We also found that the adsorption film has low adsorption performance on Fe ions, which is beneficial to the recovery of magnet boron, because magnet boron contains a lot of iron, which can make the adsorbent more accurate adsorption of Dy ions.

## 4. Conclusion

By this experiment, we compared the different adsorption properties of ion-guided graphene imprinted film and non-imprinted film on Dy ions, and successfully prepared ion-guided graphene imprinted film with high

adsorption performance and good selective adsorption performance. The film with graphene oxide is more flexible. Lastly, through the adsorption experiment, we found that at pH = 5.0, the adsorption performance of the membrane to Dy ions was the best, and the adsorption reached equilibrium after 2 h of adsorption. The maximum adsorption amount reached 26.27 mg g<sup>-1</sup>. The membrane has high acid resistance and high adsorption selectivity to Dy ions. The adsorption model is the chemical adsorption of the monolayer. Finally, there are some empirical shortcomings in the process of experiment, hoping to improve in the future experiment and research.

## References

- [1] D. Lerche, Y. Nozaki, Rare earth elements of sinking particulate matter in the Japan Trench, *Earth Planet. Sci. Lett.*, 159 (1998) 71–86.
- [2] R. Zhang, L. Wang, Y. Li, H. Li, Y. Xu, Distribution characteristics of rare earth elements and selenium in hair of centenarians living in China Longevity Region, *Biol. Trace Elem. Res.*, 197 (2020) 15–24.
- [3] K.M. Mahmoud, Y.S. Rammah, Investigation of gamma-ray shielding capability of glasses doped with Y, Gd, Nd, Pr and Dy rare earth using MCNP-5 code, *Phys. B*, 577 (2020) 411756, doi: 10.1016/j.physb.2019.411756.
- [4] A. Hastir, N. Kohli, R.C. Singh, Comparative study on gas sensing properties of rare earth (Tb, Dy and Er) doped ZnO sensor, *J. Phys. Chem. Solids*, 105 (2017) 23–34.
- [5] S.-B. Jeon, I.J. Son, B.-C. Lim, J.-M. Kim, Y.-J. Kim, T.-G. Ha, H.-S. Yoon, C.-J. Kim, K.-W. Chung, Solvent extraction of light (Pr, Nd) and medium (Tb, Dy) rare earth elements with PC88A of rare earth chloride solution from waste permanent magnet, *J. Korean Inst. Resour. Recycl.*, 27 (2018) 8–15.
- [6] M. Firdaus, M.A. Rhamdhani, Y. Durandet, W.J. Rankin, K. McGregor, Review of high-temperature recovery of rare earth (Nd/Dy) from magnet waste, *J. Sustainable Metall.*, 2 (2016) 276–295.
- [7] X. Wei, G. Xu, C. Gong, F. Qin, X. Gong, C. Li, Fabrication and evaluation of sulfanilamide-imprinted composite sensors by developing a custom-tailored strategy, *Sens. Actuators, B*, 255 (2018) 2697–2703.
- [8] X. Wei, M. Yu, C. Li, X. Gong, F. Qin, Z. Wang, Magnetic nanoparticles coated with a molecularly imprinted polymer doped with manganese-doped ZnS quantum dots for the determination of 2,4,6-trichlorophenol, *Microchim. Acta*, 185 (2018) 208, doi: 10.1007/s00604-018-2742-5.
- [9] Y.R. Smith, D. Bhattacharyya, T. Willhard, M. Misra, Adsorption of aqueous rare earth elements using carbon black derived from recycled tires, *Chem. Eng. J.*, 296 (2016) 102–111.
- [10] X. Sun, H. Luo, S.M. Mahurin, R. Liu, X. Hou, S. Dai, Adsorption of rare earth ions using carbonized polydopamine nano carbon shells, *J. Rare Earths*, 34 (2016) 77–82.
- [11] F. Li, X.-M. Li, S.-S. Zhang, One-pot preparation of silica-supported hybrid immobilized metal affinity adsorbent with macroporous surface based on surface imprinting coating technique combined with polysaccharide incorporated sol-gel process, *J. Chromatogr. A*, 1129 (2006) 223–230.
- [12] L. Qin, X.-W. He, W. Zhang, W.-Y. Li, Y.-K. Zhang, Macroporous Thermosensitive imprinted hydrogel for recognition of protein by metal coordinate interaction, *Anal. Chem.*, 81 (2009) 7206–7216.
- [13] M.R. Awual, New type mesoporous conjugate material for selective optical copper(II) ions monitoring & removal from polluted waters, *Chem. Eng. J.*, 307 (2017) 85–94.
- [14] L. Chen, S. Xu, J. Li, Recent advances in molecular imprinting technology: current status, challenges and highlighted applications, *Chem. Soc. Rev.*, 40 (2011) 2922–2942.
- [15] E. Du, J. Li, S. Zhou, L. Zheng, X. Fan, Transformation of naproxen during the chlorination process: Products identification and quantum chemistry validation, *Chemosphere*, 211 (2018) 1007–1017.
- [16] X. Wei, Z.D. Zhang, Z.H. Wang, A simple dopamine detection method based on fluorescence analysis and dopamine polymerization, *Microchem. J.*, 145 (2019) 55–58.
- [17] X. Zheng, Y. Wang, F. Qiu, Z. Li, Y. Yan, Dual-functional mesoporous films templated by cellulose nanocrystals for the selective adsorption of lithium and rubidium, *J. Chem. Eng. Data*, 64 (2019) 926–933.
- [18] X. Zheng, Y. Zhang, F. Zhang, Z. Li, Y. Yan, Dual-template docking oriented ionic imprinted bilayer mesoporous films with efficient recovery of neodymium and dysprosium, *J. Hazard. Mater.*, 353 (2018) 496–504.
- [19] E.O. Adekanmbi, A.T. Giduthuri, S. Waymire, S.K. Srivastava, Utilization of dielectrophoresis for the quantification of rare earth elements adsorbed on *Cupriavidus necator*, *ACS Sustainable Chem. Eng.*, 8 (2020) 1353–1361.
- [20] X. Zheng, Y. Zhang, T. Bian, Y. Zhang, F. Zhang, Y. Yan, Selective extraction of gadolinium using free-standing imprinted mesoporous carboxymethyl chitosan films with high capacity, *Cellulose*, 26 (2019) 1209–1219.